JMEPEG (2012) 21:2472–2479
DOI: 10.1007/s11665-012-0201-8

1059-9495/$19.00

Electrochemical Evaluation of Radiation-Induced Segregation in Austenitic Stainless Steels with Oversize Solute Addition

Parag M. Ahmedabadi, V. Kain, M. Gupta, I. Samajdar, S. Sharma, P. Bhagwat, and Y. Watanabe

(Submitted April 7, 2011; in revised form December 20, 2011)

Effect of different levels of oversize element, cerium, on radiation-induced segregation (RIS) in type 316 stainless steel was investigated. The effect of prior cold-work on RIS was also investigated. Samples with 0.00, 0.01, and 0.04 wt.% cerium were irradiated to 0.70 dpa using 4.8 MeV protons at 300 °C. Characterization of proton-irradiated specimens was carried out using electrochemical potentiokinetic reactivation (EPR) test followed by atomic force microscopic examination. The specimen with prior cold-work (without cerium addition) showed the lowest EPR values indicating the lowest chromium depletion in this material. The specimen with 0.04 wt.% cerium showed the lower EPR value as compared to the specimen with 0.01 wt.% Ce. The irradiated specimen with prior cold-work showed linear features after the EPR tests and such features were attributed to decoration of dislocations, generated due to prior cold-work, by point defects produced during irradiation. The resistance to RIS offered by cold-work (linear features) has been more effective as compared to that by the addition of oversize solute addition.

Keywords atomic force microscopy, austenitic stainless steel, cold-work, electrochemical potentiokinetic reactivation, oversize solute, proton-irradiation

1. Introduction

Neutron irradiation results in microstructural and microchemical changes in austenitic stainless steels (SS). Irradiation damage results in an increased susceptibility of austenitic SS toward irradiation-assisted stress corrosion cracking (IASCC) in light water reactors (LWR) environment. IASCC is a complex process and is influenced by microstructural and microchemical changes due to irradiation. Radiation-induced segregation (RIS) is one of the parameters (Ref 1-4) that influence IASCC in austenitic SS. RIS is the non-equilibrium segregation of alloying elements that leads to depletion of chromium at grain boundaries. It also results in segregation of silicon and phosphorus, and nickel at grain boundaries. RIS is governed by the migration of point defects toward grain boundaries; therefore, increasing point defect recombination within the matrix would help in delaying/reducing RIS at grain boundaries. The addition of oversize element in austenitic SS is one of the methods to control RIS in austenitic SS. The addition of oversize solute atoms has been shown to reduce RIS by augmenting the process of point defect recombination within the matrix (Ref 5-12). Kato et al. (Ref 9) investigated the effect of the addition of 0.35 at.% of various oversize elements like Ti, Zr, Hf, V, Nb, and Ta on both RIS and void formation in 316L SS, irradiated with electrons to 10.8 dpa at temperatures ranging from 400 to 500 °C. It was reported that RIS behavior of Cr and Ni were strongly affected by the addition of oversize solutes. The addition of Hf and Zr was found to completely suppress RIS. Further studies on same alloys (Ref 11) irradiated with fast neutrons (up to 35 dpa) in the temperature range of 425-600 °C confirmed the beneficial effect of Hf and Zr addition. Shigenaka et al. (Ref 6) performed 400 keV He^{+} irradiation on type 316L SS with addition of 0.07, 0.21, or 0.41 wt.% Zr up to 3.4 dpa. An almost complete suppression of Cr depletion at grain boundaries was noticed when the Zr content was >0.21 wt.%. Watanbe et al. (Ref 5) carried out electron irradiation studies on Fe-16Cr-17Ni pure ternary austenitic alloys doped with 0.1Nb and the beneficial effect of such an addition on radiation-induced microstructure was observed at dose up to 2 dpa. Dumbill and Hanks (Ref 12) investigated the effect of Ti (0.18 wt.%) and Nb (0.44 wt.%) on RIS of type 304 SS irradiated with 46.5 Ni^{6+} up to 5 dpa. Ti and Nb both resulted in an important reduction of the extent of RIS at grain boundaries. Kasahara et al. (Ref 7) investigated the effect of 0.32 wt.% Ti and Nb additions on IASCC of 316L SS; neither addition of Ti nor Nb was found to improve resistance to IASCC. However, Fournier et al. (Ref 13) have observed the beneficial effect of addition of oversize solute elements, Hf and Pt, on resistance of type 316L SS toward IASCC. They also found that both Hf and Pt were beneficial in suppressing/retarding RIS on grain boundaries in type 316 SS. Samples of SS were subjected to proton-irradiation and subsequently to IGSCC in a simulated BWR environment. The beneficial effect

Parag M. Ahmedabadi and **V. Kain**, Materials Science Division, Bhabha Atomic Research Centre, Trombay, Mumbai 400085, India; PEC University of Technology, Chandigarh, India; **M. Gupta**, Department of Metallurgical Engineering & Materials Science, Indian Institute of Technology Bombay, Mumbai, India; **I. Samajdar**, Nuclear Physics Division, Bhabha Atomic Research Centre, Mumbai 400085, India; and **S. Sharma, P. Bhagwat,** and **Y. Watanabe**, Department of Quantum Science and Energy Engineering, Graduate School of Engineering, Tohoku University, Sendai, Japan. Contact e-mail: id.parag@gmail.com.

of addition of oversize solute atoms was attributed to reduction in point defect migration to the grain boundary and agglomeration into loops and voids by trapping migrating vacancies and subsequently increasing the recombination rate (Ref 5-10). The formation of Hf-vacancy (Ref 13) complexes and the subsequent enhancement of point defect recombination is a plausible mechanism as it would result in a reduction in the partitioning of point defect flux to grain boundaries. Sakaguchi et al. (Ref 8) have considered that the oversize solute atoms interact with vacancies via the formation of an additive-vacancy complex. In an earlier work, it has been reported that the effect of addition of cerium in steels, on its corrosion properties, is to form a thermodynamically stable surface film composed of cerium oxide (Ref 14). This reduces the cathodic/anodic reactivity by blocking the reactive surface sites and improves resistance to pitting/crevice corrosion (Ref 14, 15). The addition of cerium is also reported to have improved the dry oxidation resistance (Ref 16, 17) of SS which was attributed to the larger atomic size of the rare earth element with respect to iron. The vacancies in the alloy move to the stressed regions adjacent to the rare earth oxides at the metal/oxide interface where they serve as nucleation sites for formation of chromium oxide and also affect the diffusion rate of chromium. SS 316 with Ce content have been shown to increase the resistance to sensitization (Ref 18) as well as IGSCC (Ref 19). It was also shown that SS 316 with Ce content up to 0.01 wt.% improves resistance to thermal sensitization as well as low temperature sensitization (Ref 18). In the present investigation, the effect of oversize solute addition on RIS has been studied in type 316 and compared with the effect of prior cold-work. Proton-irradiation at 300 °C was used to develop RIS in the material. Proton-irradiated specimens were characterized using electrochemical potentiokinetic reactivation (EPR) technique followed by atomic force microscopic (AFM) examination. The EPR was used to characterize RIS in austenitic SS (Ref 20-25). Characterization of RIS by analytical techniques reveals information about irradiation-induced microstructural and microchemical changes and electrochemical techniques yield information about the influence of irradiation-induced microstructural and microchemical changes on the corrosion characteristics of the material (Ref 23).

2. Material and Experimental

2.1 Material and Processing

Type 316 SS with Ce additions of 0.01 and 0.04 wt.% was selected and another type 316 SS without Ce addition (but with residual cold-work) was also chosen for the comparison. The chemical composition of type 316 SS with different Ce contents are given in Table 1 and all specimens were used in the as-received conditions without further processing. Specimens used for proton-irradiation were electropolished in 90% methanol, 10% perchloric acid solution at a temperature < -30 °C to remove surface deformation generated due to mechanical grinding and polishing.

2.2 Proton-Irradiation

Proton-irradiation was performed using a specifically designed assembly at PELLETRON accelerator, a joint Bhabha Atomic Research Centre-Tata Institute of Fundamental Research (BARC-TIFR) facility. The experimental doses and dose rates were calculated using SRIM (Ref 26), while accumulated irradiation damage due to proton-irradiation, in terms of dpa, was estimated using the NRT equation (Ref 27):

$$\mathrm{dpa} = \frac{0.8}{2E_\mathrm{d}}\left(\frac{\mathrm{d}E}{\mathrm{d}x}\right)_n \frac{\varphi_t}{\rho}, \qquad \text{(Eq 1)}$$

where E_d is the displacement energy, $(\mathrm{d}E/\mathrm{d}x)n$ is the linear energy transfer (LET) per ion to target by nuclear processes, φ_t is the fluence per unit area, and ρ is the atomic density. $(\mathrm{d}E/\mathrm{d}x)_n$ was obtained from SRIM by summing up phonon and binding energy profiles. The displacement energy is the energy required to displace the target atom from its lattice position and it is taken as 40 eV (Ref 26) in the present investigation. The binding energy profile was obtained by vacancy profile multiplied by binding energy (=3 eV) used in SRIM calculations. The dose rate during proton-irradiation experiments was 2.768×10^{-6} dpa/s (displacement per atom/second). The typical surface area which was irradiated for each specimen was around 7 mm^2. The specimen temperature during experiment was maintained at 300 ± 5 °C and the level of vacuum was maintained at 1.3×10^{-5} $\mathrm{N/m}^2$. The damage profile obtained using SRIM for proton-irradiation was given a curve-fitting using the following equation (4-parameter Pseudo-Voigt equation)

$$y = a\left[\frac{c}{1+\alpha^2} + (1-c)\exp\left(-0.5\alpha^2\right)\right], \qquad \text{(Eq 2)}$$

where $\alpha = (x - x_0)/b$ and a, b, c are constants, x is depth, and y is the damage corresponding to given x.

2.3 Double Loop EPR

The extent of chromium depletion in irradiated type 316 SS specimens and was characterized using the DL-EPR technique. It is known that the passive film on type 316 SS is more stable as compared to that on type 304 SS (Ref 28), hence, a more aggressive test solution was used in the EPR test to evaluate the extent of Cr depletion in sensitized and irradiated specimens. The DL-EPR test was carried out (Ref 29) in a solution of 1.0 mol/L H_2SO_4 and 0.1 mol/L KSCN (deaerated) at room temperature. The potential was scanned from −30 mV versus open circuit potential (OCP) to +300 $\mathrm{mV_{SCE}}$ (vs. saturated calomel electrode) and then back to OCP at a scan rate of 6 V/h. The non-irradiated area on each specimen was masked with lacquer and only the irradiated area was exposed during

Table 1 Chemical composition, grain size, and hardness of type 316 SS with different Ce contents

Element	C	Si	Mn	*P*, ppm	*S*, ppm	Ni	Cr	Mo
Ce 0.00	0.058	0.54	1.20	<5	20	13.02	16.92	2.22
Ce 0.01	0.066	0.54	1.20	<5	40	12.84	16.84	2.22
Ce 0.04	0.065	0.55	1.20	<5	20	13.11	16.91	2.24

the DL-EPR test. The degree of sensitization (DOS) is reported as the DL-EPR value which is the ratio of current in the backward (reactivation) loop to that in the forward (anodic) loop, multiplied by 100. The maximum damage due to proton-irradiation occurs at approximately 70 μm (Ref 11) below the surface for proton energy of 4.8 MeV. Therefore, starting from the as-irradiated surface, the DL-EPR test was repeated after removing the affected layer after each test, until the non-irradiated material was reached. After each DL-EPR test, the affected layer was removed using fine emery-paper grinding followed by polishing with 0.5 μm diamond paste.

2.4 AFM Examinations

After each DL-EPR test, the specimen was characterized using NT-MDT Solver Pro scanning probe microscope in AFM mode in air using semi-contact mode. The AFM scans were done on a 12 × 12 μm area and a number of scans were done for each condition of specimen. The extent of attack was measured as depth of attack after DL-EPR using AFM on various microstructural features like grain boundaries and twin boundaries and any other feature within grains.

3. Results

3.1 Electrochemical Characterization

Figure 1(a) shows variation of damage due to 4.8 MeV protons with the depth as calculated by SRIM for 0.7 dpa. As depicted in the graph, the damage profile for proton-irradiation of 4.8 MeV energy consists of a region of uniform damage region for nearly first 70 μm of depth followed by a region of peak damage up to depth of 80 μm. For 0.70 dpa, the average damage in the region of uniform damage was 0.05 dpa and in the peak damage region was 0.285 dpa. Figure 1(a) also depicts results of DL-EPR test for specimen irradiated to 0.70 dpa with respect to depth. The maximum damage (DL-EPR value) was found at the depth of 40, 80, and 70 μm for 0.00, 0.01, and 0.04 wt.% Ce, respectively. The variation in DL-EPR values with the depth showed a trend similar to that from SRIM predictions. Except for SS 316 with Ce 0.00 wt.%, the depth of maximum damage matched with the prediction of the peak damage area by SRIM for 4.8 MeV protons in type 304 SS; with SRIM prediction that the peak damage area lies at a depth of 70 and 80 μm. The extent of damage (in terms of DOS) versus depth was given a curve-fit using Eq 2 and plotted simultaneously in Fig. 1(a). The average and maximum DOS values are depicted Fig. 1(b). Type 316 SS with Ce 0.00 wt.% showed the lowest average and maximum DL-EPR values among all the specimens.

3.2 Microscopic Examination

The microstructures developed on the as-irradiated surface for type 316 SS with Ce 0.00, 0.01 and 0.04 wt.% did not show typical austenitic grain structure. This could probably be due to structural modification of the as-irradiated surface as the top most layer of the irradiated specimen acts as an effective sink for irradiation induced defects. This indicates that the as-irradiated surfaces got heavily attacked during the DL-EPR tests. Figure 2 depicts optical micrographs at the depth where maximum DL-EPR value was obtained. Figure 2(a) shows an optical micrograph of type 316 SS with Ce 0.00 wt.% after the

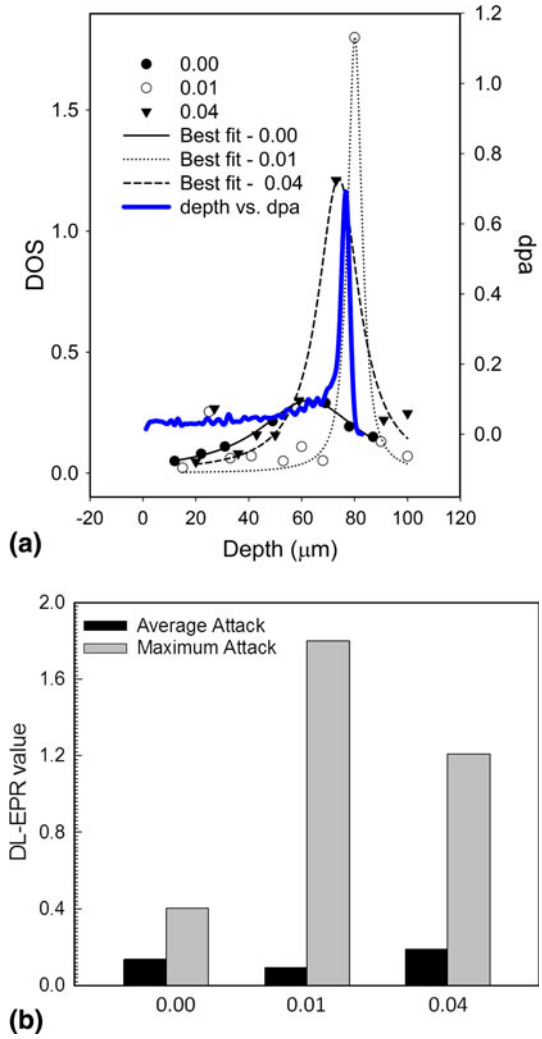

Fig. 1 Graphical representation of irradiation damage in type 316 SS specimens with different Ce contents and irradiated to 0.70 dpa showing (a) variation in proton-irradiation damage and DL-EPR values with depth and (b) average and maximum DOS values

DL-EPR test at the depth of 50 μm, illustrating strain-markings and pit-like features within grains. Figure 2(b) depicts an optical micrograph for type 316 SS with Ce 0.01 wt.% after DL-EPR at the depth of 80 μm, showing attack at a few grain boundaries and a few pit-like features within grains. No strain-markings were observed for this specimen. Similar observations made for type 316 SS with Ce 0.04 wt.% and optical micrograph is depicted in Fig. 2(c). SEM micrographs of irradiated type 316 SS specimens with different Ce contents are depicted in Fig. 3. All micrographs shown were obtained after the DL-EPR tests at the depth of maximum DL-EPR values. Figure 3(a) shows an SEM micrograph for 0.00 wt.% Ce after DL-EPR at depth of 50 μm. Strain-markings and pit-like features within grains were noticed and attack on grain boundary was negligible. Figure 3(b) and (c) represents SEM micrographs for 0.01 and 0.04 wt.% Ce, respectively. The microstructural features for both specimens were similar in nature; attack on grain boundaries and twin boundaries were noticed and a few pit-like features were noticed within grains. No strain-markings were noticed for the specimens with 0.01 and 0.04 wt.% Ce. The attack on a few twin boundaries was

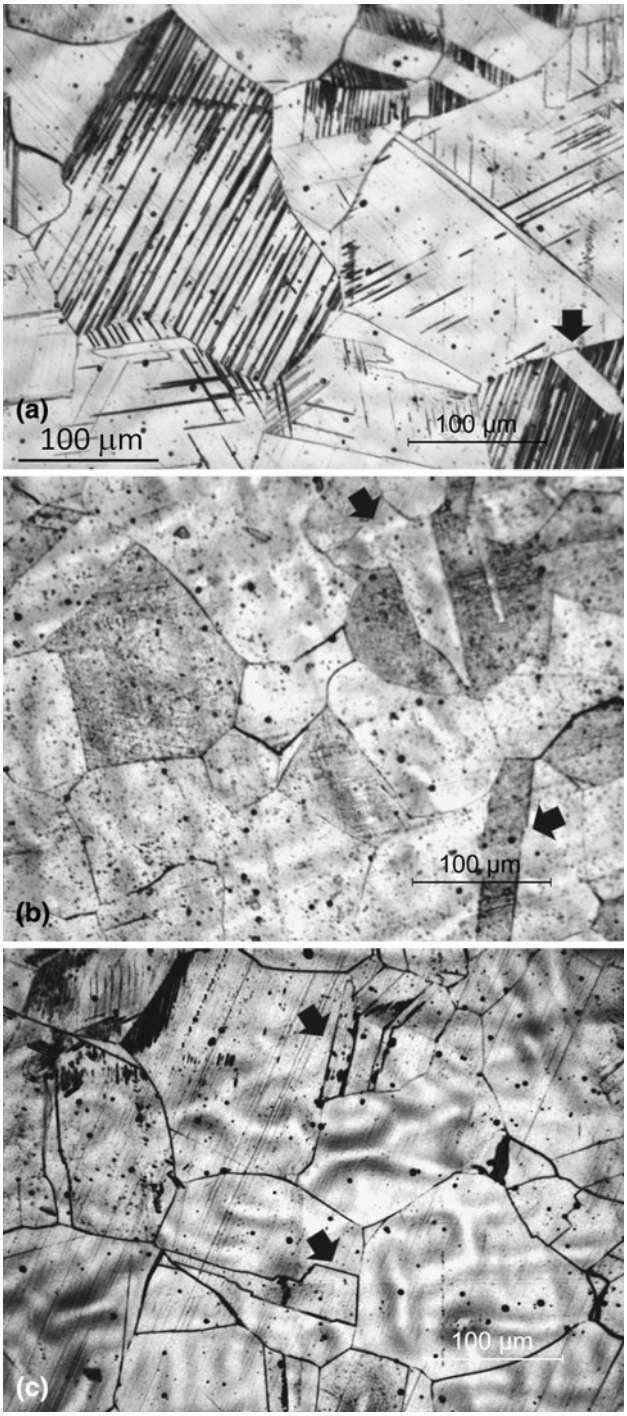

Fig. 2 Optical micrographs of type 316 SS with different Ce contents after DL-EPR at depths where maximum DL-EPR was obtained, illustrating (a) strain-markings and pit-like features within grains, (b) attack on grain boundaries and pit-like features within grains, and (c) attack on grain boundaries and pit-like features within grains. The arrows indicate twin boundaries within the matrix

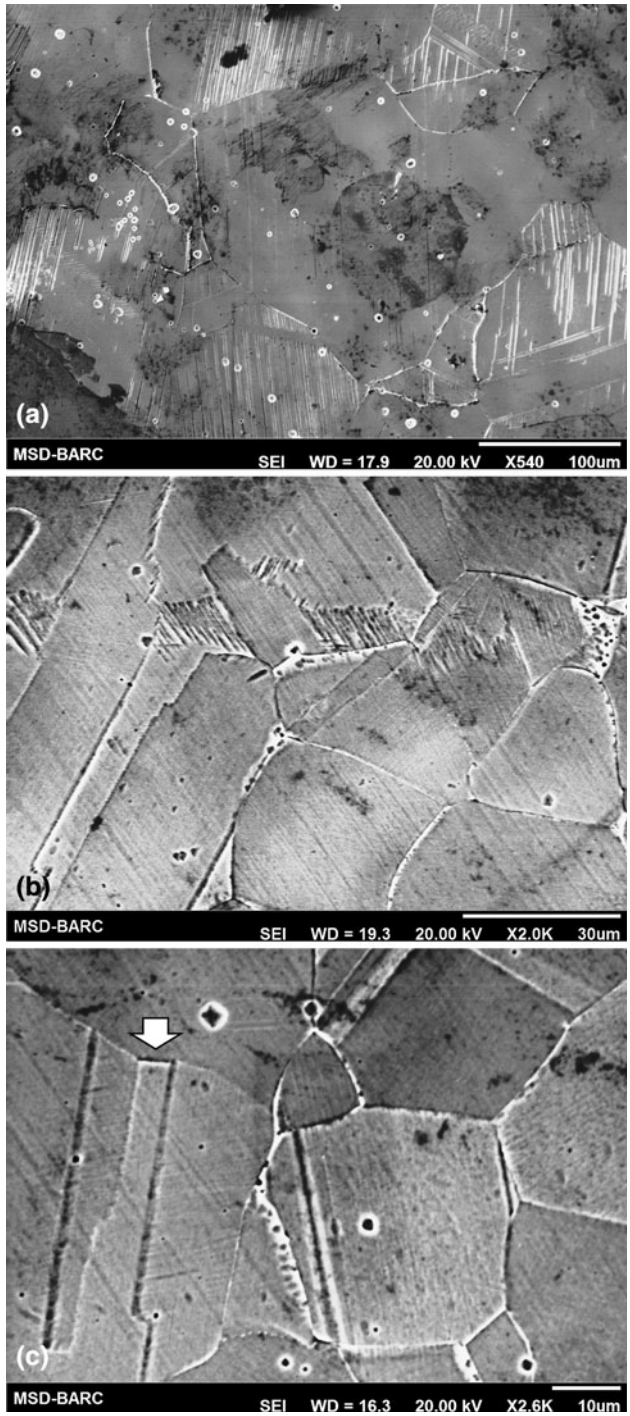

Fig. 3 SEM micrographs of irradiated type 316 SS with different Ce contents after DL-EPR at depths where maximum damage was noticed illustrating (a) for type 316 SS with Ce 0.00 wt.%, showing attack on strain-markings and on pit-like features within grains, (b) for type 316 SS Ce 0.01 wt.%, showing attack on grain boundaries, twin boundaries and on pit-like features within grains, and (c) irradiated SS 316 Ce 0.04 wt.%, microstructural features were similar to that of SS 316 Ce 0.01 wt.%

also noticed and intersection of a twin boundary with a grain boundary also got attacked as shown by an arrow in Fig. 3(c).

3.3 AFM Examination

Figure 4 shows AFM micrographs of irradiated (0.70 dpa) type 316 SS specimens with different Ce contents. All AFM images depicted in Fig. 4 were obtained at the depth of the maximum DL-EPR value for each specimen. The depth of attack on linear features within the matrix for 0.00 wt.% Ce specimen is illustrated in Fig. 4(a), the depth of attack varied in the range of 100-250 nm. Figure 4(b) depicts an AFM image

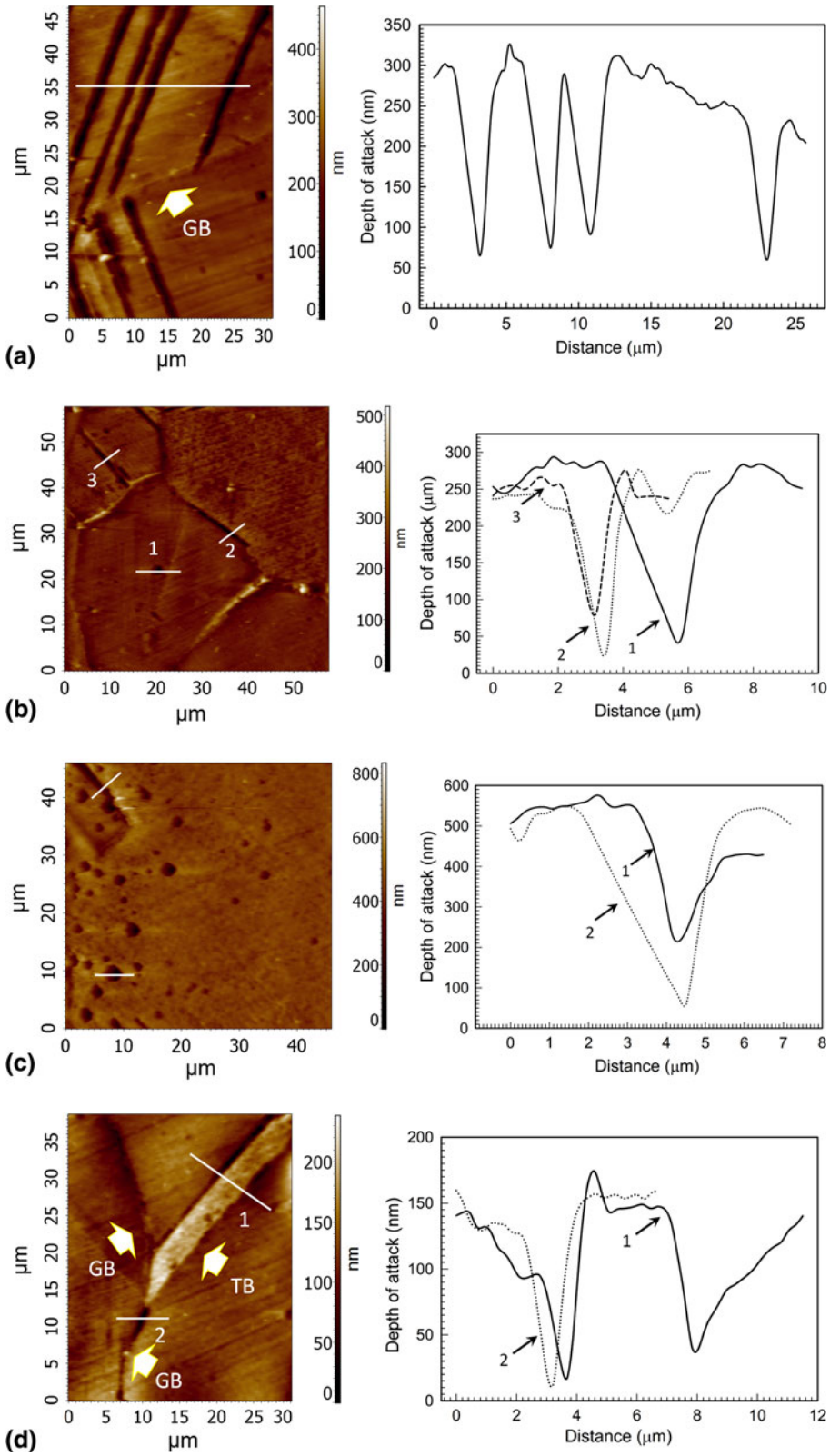

Fig. 4 SEM micrographs of irradiated type 316 SS with different Ce contents after DL-EPR at depths where maximum damage was noticed illustrating (a) for type 316 SS with Ce 0.00 wt.%, showing attack on strain-markings and on pit-like features within grains, (b) for type 316 SS Ce 0.01 wt.%, showing attack on grain boundaries, twin boundaries, (c) on pit-like features within grains, and (d) irradiated type 316 SS Ce 0.04 wt.%, microstructural features were similar to that of SS 316 Ce 0.01 wt.%

for the specimen with 0.01 wt.% Ce, showing attack at three different locations on three different microstructural features viz. a grain boundary, a pit-like feature within the matrix, and a twin boundary. The depth of attack at these locations (Location 1 to 3 in Fig. 4b) varied between 150 and 250 nm. Figure 4(c) depicts several pit-like features within the matrix and attack on a twin boundary in the specimen with 0.01 wt.% Ce. The depth of attack on pit-like features was in the range of 150-450 nm and on the twin boundary shown in the image was ~250 nm. The attack on twin boundaries and grain boundaries in the specimen with 0.04 wt.% is shown in Fig. 4(d). The intersection of a grain boundary and a twin boundary remained unaffected as shown in the figure. The depth of attack on a twin and grain boundary was ~150 nm. It may be noted that the intersection of a twin boundary with a grain boundary remained unaffected in Fig. 4(d) whereas, in Fig. 3(c), the intersection of a twin and grain boundary got attacked. No linear features were noticed for the specimens with 0.01 and 0.04 wt.% Ce. Moreover, the fraction of grain boundaries and twin boundaries that got attacked during the DL-EPR tests was more for the specimen without prior cold-work, i.e., 0.01 and 0.04 wt.% Ce. It may be noted that the fractions of twin boundaries and grain boundaries got attacked during the DL-EPR were negligible for the specimen with 0.00 wt.% Ce. The fraction of grain boundaries that got attacked after the DL-EPR tests was 20 and 15% for 0.01 and 0.04 wt.% Ce, respectively. The fraction of twin boundaries that got attacked during the DL-EPR test for Ce-containing alloys was less as compared to the fraction of attacked grain boundaries and the fraction was of the order of 2-3%.

4. Discussion

The variation of DL-EPR value with depth follows similar trend as that of damage versus depth as predicted by SRIM for SS 316 with 0.01 and 0.04 wt.% Ce and the maximum damage was observed in the range of 70 to 80 μm. This was not the case for SS 316 with 0.00 wt.% Ce and the maximum damage (indicated by the DL-EPR value) was noticed at 50 μm for this sample. This may be due to the presence of many defect sinks within the matrix, the presence of strain-markings might have altered rate of point defects recombination and annihilations. The SRIM calculation does not take into account crystal structure and various defect sinks present in the material. The relative effect of addition of various oversize elements on RIS in austenitic SS was modelled (Ref 8) using the linear size factor and is defined as (in %):

$$L_{sf} = \left(\left(\frac{\Omega_{add}}{\Omega_{sol}} \right)^{1/3} - 1 \right) \times 100, \qquad \text{(Eq 3)}$$

where Ω_{sol} is the atomic volume of the solvent and Ω_{add} is the atomic volume of additive. Calculated linear size factor for various oversize solute atoms (Ref 9) are given in Table 2. Model predictions were in good agreement with RIS measurements performed by Kato et al. (Ref 9) on model 316L SS doped with different oversize elements. It can be seen from the Table 1 that cerium atom has the highest linear size factor among all elements depicted. The atomic radii of cerium and iron are 1.83 and 1.24 A°, respectively (Ref 30). The atomic volumes of cerium and iron are 20.67 and 7.1 cm^3/mol, respectively (Ref 30). Thus, the size and the volume of cerium atom are larger than that of the iron atom. This would result in more strain energy at the boundary of the cerium atom and the austenitic lattice (Ref 18, 19). The linear size factor for the cerium atom is also very high as compared to other elements as listed in Table 2. Thus, it is expected that higher strain energy within the grains (matrix) due Ce addition would provide more effective hindrance to migration of point defects toward grain boundaries. DL-EPR results have indicated that the extent of RIS in SS 316 with 0.00 wt.% Ce was less as compared with the 0.01 and 0.04 wt.% Ce. Type 316 SS with 0.00 wt.% Ce had strain-markings within the matrix can act as sinks for point defects. The attack on strain-regions within the matrix during the DL-EPR tests appeared as linear features under microscopic examination. Linear features are manifestation of deformation microstructure in low stacking fault energy (SFE) material type 316 SS. The deformation microstructure in low SFE materials like 304 and 316 SS consists (Ref 31, 32) of array of dislocations on {111} slip-planes, micro-twins, and/or deformation-induced martensite. All these microstructural features appeared as linear indications during microscopic examinations and are regions of higher strain energy. Such regions can act as sinks for point defects generated during irradiation leading to point defect recombination and/or chromium depletion by inverse Kirkendall mechanism. Type 316 SS with 0.01 and 0.04 wt.% Ce showed attack on grain boundaries and twin boundaries after DL-EPR tests. It indicates that in the absence of strained regions within the matrix, point defects moved to grain boundaries and twin bound-aries. This led to chromium depletion at grain boundaries and twin boundaries due to inverse Kirkendall mechanism. The attack on twin boundaries were also observed (Ref 33, 34) after DL-EPR tests in proton-irradiated type 304 SS specimens. The attack on twin boundaries in the present investigation confirms previous observations that twin boundaries can also act as defect sinks, however, the extent of RIS is expected to be less as compared to that at random boundaries due to less available free energy. Grain boundaries and twin boundaries provide less surface area as compared to strain-markings within grains and hence, DL-EPR values were higher for type 316 SS with 0.01 and 0.04 wt.% Ce. Therefore, strain-regions within the matrix due to prior cold-work reduce flux of point defects toward grain boundaries and twin boundaries. The addition of oversize solute atoms produces strained regions in localized regions surrounding oversize solute atoms whereas strain-markings (due to prior cold-work) produces strain-regions over a large surface on slip planes. It implies that strain-regions due to prior cold-work are more effective sinks

Table 2 Calculated linear size factor for various oversize solute elements

Element	Atomic number	Atomic volume, cm^3	L_{sf}, %
V	20	8.36	6.81
Pt	78	9.09	9.84
Ti	22	10.62	15.68
Nb	41	10.83	16.44
Ta	73	10.85	16.51
Zr	40	14.01	26.87
Hf	72	13.41	25.04
Ce	58	20.67	42.78

as compared to the addition of oversize solute elements. In view of presence of strain-regions within the matrix, type 316 SS with 0.00 wt.% Ce showed lesser attack during DL-EPR, indicating less RIS due to proton-irradiation. The specimen with 0.04 wt.% Ce showed lower DL-EPR values (average and maximum) than the specimen with 0.01 wt.% Ce. Similar observations were made in an earlier investigation on the same specimens irradiated to 0.43 dpa (Ref 35). A few pit-like features were noticed within grains for SS 316 with 0.01 and 0.04 wt.% Ce, that might correspond to strain-regions surrounding cerium atoms within matrix. It is also possible that such pit-like features might have appeared due to attack on dislocation loops. Chromium depletions were reported within the matrix and migration of vacancies to dislocation loops may lead to chromium depletion in dislocation regions. Pit-like features within the matrix were also reported (Ref 23, 25) in previous investigation after the EPR tests on irradiated austenitic SS. The strain-fields around dislocation loops are of the order of nano-meter. However, due to corrosive attack during DL-EPR test on chromium depletion regions (surrounding dislocation loops), pit-like features of the order of micrometer formed. Similar observations were made in previous investigations (Ref 23, 25, 33) that used EPR technique to characterize RIS in austenitic SS.

5. Conclusions

The effects of oversize solute addition and prior cold-work on RIS were investigated using proton-irradiation. Type 316 SS with 0.00, 0.01, and 0.04 wt.% Ce were irradiated to 0.70 dpa using 4.8 MeV protons. The extent of RIS in proton-irradiated was characterized using EPR test followed by microstructural examination using scanning electron microscope (SEM) and AFM. Following are the conclusions derived from the present investigation.

1. The results of DL-EPR had indicated that the presence of strain-markings (residual strain) was more effective in reducing chromium depletion regions at grain boundaries as compared to addition of oversize solute additions.
2. The specimen with 0.04 wt.% Ce showed lower maximum DL-EPR value as compared to the specimen with 0.01 wt.% Ce, showing effectiveness of Ce addition in increasing the resistance against RIS.

References

1. A. Etienne, M. Hernàndez-Mayrol, C. Genevois, B. Radiguet, and P. Parieige, Dislocation Loop Evolution Under Ion Irradiation in Austenitic Stainless Steels, *J. Nucl. Mater.*, 2010, **400**, p 56–63
2. Z. Jiao, J.T. Busby, and G.S. Was, Deformation Microstructure of Proton-Irradiated Stainless Steels, *J. Nucl. Mater.*, 2007, **361**, p 218–227
3. P.L. Andresen, F.P Ford, S.M. Murphy, J.M. Perks, *Proc. of the 4th International Symposium on Environmental Degradation of Materials in Nuclear Power Systems-Water Reactors*, NACE International, Houston, 1990
4. M.J. Hackett, R. Najafabadi, and G.S. Was, Modeling Solute-Vacancy Trapping at Oversized Solutes and its Effect on Radiation-Induced Segregation in Fe-Cr-Ni Alloys, *J. Nucl. Mater.*, 2009, **389**, p 279–287
5. H. Watanbe, T. Muroga, and N. Yshida, The Effects of Oversized Solute Addition on Microstructural Evolution in Fe-Cr-Ni Alloys During Electron Irradiation, *J. Nucl. Mater.*, 1996, **239**, p 95
6. N. Shigenaka, S. Ono, Y. Isobe, T. Hashimoto, H. Fujimori, and S. Uchida, Effect of Zirconium Addition to Austenitic Stainless Steels on Suppression of Radiation Induced Chromium Segregation at Grain Boundaries under Ion Irradiation, *J. Nucl. Sci. Technol.*, 1996, **33**, p 577
7. S. Kasahara, K. Nakata, K. Fukuya, S. Shima, A.J Jacobs, G.P. Wozadlo, and S. Suzuki, *Proc. of the Sixth International Symposium on Environmental Degradation of Materials in Nuclear Power, Systems Water Reactors*, 15 August, San Diego, CA, The Minerals, Metals and Materials Society, 1993, p 615
8. N. Sakaguchi, S. Watanabe, and H. Takahashi, Effect of Additional Minor Element on Radiation-Induced Grain Boundary Segregation in Austenitic Stainless Steel Under Electron Irradiation, *Nucl. Instrum. Methods B*, 1999, **153**, p 142
9. T. Kato, H. Takahashi, and M. Izumiya, Grain Boundary Segregation Under Electron Irradiation in Austenitic Stainless Steels Modified With Oversized Elements, *J. Nucl. Mater.*, 1992, **189**, p 167
10. M.A. Ashworth, D.I.R. Norris, and I.P. Jones, Radiation-Induced Segregation in Fe-20Cr-25Ni-Nb Based Austenitic Stainless Steels, *J. Nucl. Mater.*, 1992, **189**, p 289
11. S. Ohnuki, S. Yamashita, H. Takahashi, and T. Kato, *Proc. of the 19th Inter-national Symposium on the Effects of Radiation on Materials*, 16-18 June, Seattle, WA American Society for Testing and Materials, 1999, p 756
12. S. Dumbill, and W. Hanks, *Proc. of the Sixth International Symposium on Environmental Degradation of Materials in Nuclear Power Systems Water Reactors*, 15 August, San Diego, CA, The Minerals, Metals and Materials Society, 1993, p 521
13. L. Fournier, B.H. Sencer, G.S. Was, E.P. Simonen, and S.M. Bruemmer, The Influence of Oversized Solute Additions on Radiation-Induced Changes and Post-Irradiation Intergranular Stress Corrosion Cracking Behavior in High-Purity 316 Stainless Steels, *J. Nucl. Mater.*, 2003, **321**, p 192–209
14. Y.C. Lu and M.B. Ives, The Improvement of the Localized Corrosion Resistance of Stainless Steel by Cerium, *Corros. Sci.*, 1993, **39**, p 1773
15. Y.C. Lu and M.B. Ives, Chemical Treatment With Cerium to Improve the Crevice Corrosion Resistance of Austenitic Stainless Steels, *Corros. Sci.*, 1995, **37**, p 145
16. Y. Nakamura, The Oxidation Behavior of an Iron-Chromium Alloy Containing Yttrium or Rare Earth Elements Between 900 and 1200°C, *Metall. Trans.*, 1974, **5**, p 909
17. Y. Saito, T. Kiryu, T. Kimura, T. Amano, and K.J. Yajima, *Jpn. Inst. Met.*, 1975, **39**, p 1110
18. Y. Watanabe, V. Kain, T. Tonozuka, T. Shoji, T. Kondo, and F. Masuyama, Effect of Ce Addition on the Sensitization Properties of Stainless Steels, *Scripta Mater.*, 2000, **42**, p 307–312
19. Y. Watanabe, T. Tonozuka, T. Shoji, and T. Kondo, Corrosion 99, Paper No. 453 (1999), p 1–10
20. O. Okada, K. Nakata, and S. Kasahara, Effects of Thermal Sensitization on Radiation-Induced Segregation in Type 304 Stainless Steel Irradiated With He-Ions, *J. Nucl. Mater.*, 1999, **265**, p 232–239
21. K. Kondou, A. Hasegawa, K. Abe, V. Kain, and Y. Watanbe, *Proc. of 10th International Conference on Degradation of Materials in Nuclear Power Systems-Water Reactors*, Paper No. 66, Nevada, American Nuclear Society and National Association of Corrosion Engineers, August 1991
22. R. Katsura and S. Nishimura, The NACE Annual Conference and Corrosion Show, Paper No. 91, Corrosion 92, 1992
23. G.E.C. Bell, T. Inazumi, E.A. Kenik, and T. Kondo, Effect of Additional Minor Element on Radiation-Induced Grain Boundary Segregation in Austenitic Stainless Steel Under Electron Irradiation, *J. Nucl. Mater.*, 1992, **187**, p 170–179
24. P. Ahmedabadi, V. Kain, K. Arora, and I. Samajdar, Effect of Residual Strain on RIS in Type 304 SS, *Corros. Sci.*, 2011, **53**, p 1465–1475
25. K. Kondou, A. Hasegawa, and K. Abe, Study on Irradiation Induced Corrosion Behavior in Austenitic Stainless Steel Using Hydrogen-Ion Bombardment, *J. Nucl. Mater.*, 2004, **329–333**, p 652–656
26. J.F. Ziegler and J.P. Biersack, *SRIM2003 Program*, IBM Corp, Yorktown, NY, 2003
27. M.J. Norgett, M.T. Robinson, and I.M. Torrens, A Proposed Method of Calculating Displacement Dose Rates, *Nucl. Eng. Des.*, 1975, **33**, p 30
28. R. Babić and M. Metikoš-Huković, Semiconducting Properties of Passive Films on AISI, 304 and 316 Stainless Steels, *J. Electroanal. Chem.*, 1993, **358**(1–2), p 143–160

29. V. Kain and Y. Watanabe, Development of a Single Loop EPR Test Method and its Relation to Grain Boundary Microchemistry for Alloy 600, *J. Nucl. Mater.*, 2002, **302**, p 49–59
30. Periodic table of the elements, Introduction solid-state chemistry, MIT web-site. http://web.mit.edu/course/3/3.091/www3/pt/Ce.html and http://web.mit.edu/course/3/3.091/www3/pt/Fe.html
31. W. Karlsen, K. Dohi, and T. Onchi, *Proc. of 13th International Conference on Environmental Degradation of Materials in Nuclear Power System-Water Reactors*, CNS-SNC, 2007
32. D.N. Wasnik, I.K. Gopalkrishnan, J.V. Yakhami, V. Kain, and I. Samajdar, Cold Rolled Texture and Microstructure in Types 304 and 316L Austenitic Stainless Steels, *ISIJ Int.*, 2003, **43**, p 1581–1589
33. P. Ahmedabadi, V. Kain, K. Arora, I. Samajdar, S. Sharma, and P. Bhagwat, The Role of Niobium Carbide in Radiation Induced Segregation Behaviour of Type 347 Austenitic Stainless Steel, *J. Nucl. Mater.*, 2011, **416**, p 335–344
34. P. Ahmedabadi, V. Kain, K. Arora, I. Samajdar, S. Sharma, S. Ravindra, P. Bhagwat, and R.K. Chowdhury, Radiation-Induced Segregation in Austenitic Stainless Steel Type 304: Effect of High Fraction of Twin Boundaries, *Mater. Sci. Eng. A*, 2011, **528**, p 7541–7551
35. P. Ahmedabadi, V. Kain, G.K. Dey, I. Samajdar, S.C. Sharma, P. Bhagwat, and S. Kailas, *International Topical Meeting on Nuclear Research Applications and Utilization of Accelerators*, Vienna; 4 May 2009 through 8 May 2009; Code 84190